C103-E155

SHIMADZU
Excellence in Science

FTIR TALK LETTER

Vol. 44

The garden of Kyoto's Heian Shrine includes a "hashi dono" covered bridge that provides a spectacular view of the garden.

Far-Infrared Fourier Transform Infrared Spectroscopy (Far-IR FTIR) for Observation of the Status of Zeolite Cations

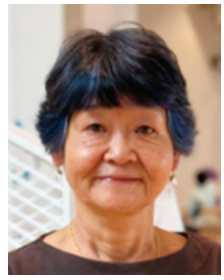

DEI Section, Office of Communications and DEI, Institute of Science Tokyo
Junko Nomura

A far-infrared (< 400 cm^{-1}) spectrum of solid oxides was successfully measured using a commercially available FTIR system, without using a synchrotron light source or special liquid helium cooled detector. Specifically, in addition to measuring the vibration between alkaline metals and lattice oxygens in cation-exchanged zeolites, in-situ measurements were attempted to confirm the adsorption/desorption behavior of molecular cations (ammonium and pyridinium cations). This article describes the results obtained as well as the "uniqueness of zeolites as a solid acid catalyst," based on the accumulated knowledge.

1. Introduction

In general, FTIR systems are used in the mid-infrared (IR) region (wavenumbers from 4600 to 400 cm^{-1}), whereas higher frequencies are referred to as the near-IR region (20000 to 4600 cm^{-1}) and lower frequencies referred to as the far-IR region (400 to 50 cm^{-1}). Mid-IR spectra show absorption from the fundamental vibrations of molecules and are used in a wide variety of research fields, whereas near-IR spectra include overtones and combinations of fundamental vibrations, serving as a tool for component analysis or quality control in a diverse range of fields, including food and agriculture. On the other hand, far-IR spectroscopy enables observation of extremely weak interaction energies. For example, when molecules in the gas phase are adsorbed on a solid surface, they lose their translational and rotational degrees of freedom, which in turn appears as three types of vibration [1, 2] originating from the motions illustrated in Fig. 1. Absorption of vibrational energies caused by such weak interactions, referred to as "adsorption," appears in far-IR spectra. Consequently, far-IR spectra provide a more direct and ideal way to investigate the strength of interactions between active sites on solid catalysts and the molecules in comparison with the conventional method of measuring internal vibrations of probe molecules (such as the CO-stretching vibration of the adsorbed CO molecule shown in Fig. 1). Nevertheless, for a variety of reasons, this technique has been seldom used (explained further below).

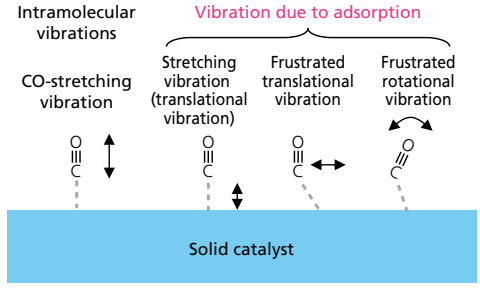

Fig. 1 Vibration Modes of Adsorbed CO

Zeolites are porous crystalline materials consisting mainly of silica (SiO_2) and aluminosilicates, where some of the silicon (Si) atoms are replaced with aluminum (Al), represented by H-ZSM-5, and are utilized as typical solid acid catalysts in the petrochemical industry. Infrared IR spectroscopy can clearly measure the protons present in oxygen (O) bridging to Al and Si as acidic hydroxyl (OH) groups at around room temperature (Fig. 2). In research on solid catalysis, IR spectroscopy has provided researchers with information on detailed observation of interactions between acidic OH groups and adsorbed molecules [3-5], reactions of adsorbed molecules via proton transfer from acidic OH groups [6, 7], and overall reaction mechanisms [8-10]. During the series of research works, the author has focused on the differences of zeolites from other metal oxides in acid catalysed reactions, the proton-hopping behavior of zeolites at high temperatures [11] and the basici-

ty of lattice oxygens next to Al that do not participate in the formation of acidic OH groups [12]. Based on those results, it was hypothesized that charges would be delocalized due to their microporous structure. In fact, early zeolite researchers have suggested that zeolites form covalent bonds as acidic OH groups when the cations are H^+ but that alkali metal cations are stabilized by the delocalized negative charge over the lattice oxygens. To clarify this point, direct measurement of the bonds between alkali cations and lattice oxygens was attempted [13] in the same manner as measuring OH groups in protonic zeolites. However, because the vibration between alkali metals and lattice oxygens is known to appear in the far-IR region, it was a challenge, which could not be confirmed with simple modifications.

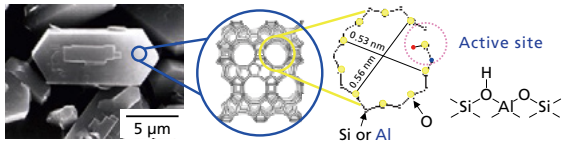

Fig. 2 SEM Image, Crystalline Structure, and Active Site of H-ZSM-5 Zeolite

2. Reason for the Difficulty of Far Infrared Spectra Measurement in the Field of Solid Catalysts

The density of active species (such as acidic OH groups) and adsorption species on solid catalysts in the beam path of FT-IR signal light is far lower than that of gas or liquid samples. Thus, multiple modifications are required even for measurements in the usual mid-IR region. Far-IR spectroscopy is far more difficult due to the low brilliance of the light sources used and the high initial and operation costs of adequate detectors for the far-IR region. For example, as compared in Fig. 3 [14], when a regular thermal light source is heated to 1127 ˚C, it generates light in the mid-IR region. Some improved light sources even generate trace amounts of light in the far-IR region. To overcome this problem, synchrotron light sources have been used to measure solid surface species in the far-IR region. Brilliance can be dramatically increased by using synchrotron radiation light, but it requires adding equipment of the measurement system, such as an atmospherically controllable closed vacuum system or temperature-variable cell, into the measurement space. In addition, conventional semiconductor detectors (MCT, InSb, etc.) do not possess adequate sensitivity, so a thermally excited TGS detector is normally used. However, due to the inadequate sensitivity of TGS detectors for measuring solid surface species, an expensive liquid helium-cooled Ge:Cu [1] or Si bolometer [2] detector is used. Not only the bolometer itself but also the liquid helium cooling experiments are extremely expensive.

Far-IR spectroscopy was first applied to a solid surface species for the observation of CO adsorbed to the metal single crystal surfaces mentioned above, with a synchrotron light source and bolometer detector. Generally, when IR light is reflected from a metal surface with an extremely large incident angle, absorption efficiency is increased dramatically to enable high-sensitivity measurements by infrared reflection absorption spectroscopy (IRAS) [15, 16]. Therefore, a small number of molecules present in the surface area of a few square millimeters, where the light is reflected, can be measured with sufficient sensitivity. For far-IR spectroscopy, the setup indicated above must be configured to use that technique. Consequently, unlike smooth metal surfaces, it is considered difficult to use far-IR spectroscopy for measuring adsorption species on powdered catalysts, for which there is no method available to achieve high sensitivity. On the other hand, it is not the case for catalysts with microporous structures possessing surface area that is orders of magnitude larger. The first zeolite samples measured by far-IR spectroscopy were sodium type ZSM-5 and mordenite single crystals [17, 18], where structures were analyzed by extended X-ray absorption fine structure (EXAFS) in combination with theoretical calculations [17, 19], using a variety of light sources but a Si bolometer detector for all measurements.

Direct measurement of interactions between solid surfaces and adsorbed molecules is an extremely essential and intriguing topic for catalyst research. Therefore, results from the following research are presented below to demonstrate the method of far-IR spectroscopy using a general FT-IR system without any special equipment and to show that it is possible.

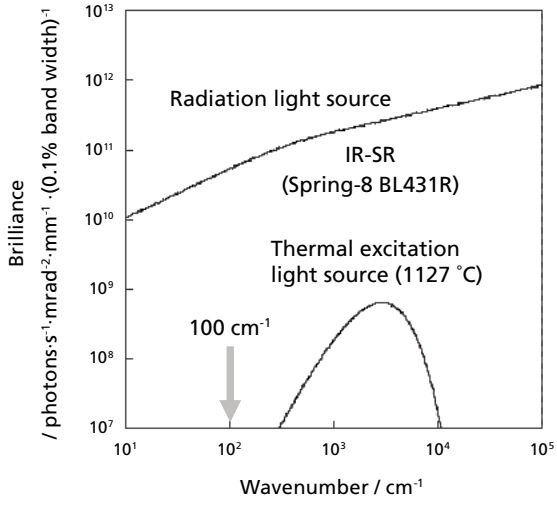

Fig. 3 Comparison of Brilliance of Synchrotron Radiation and Thermal Excitation Light Sources

3. In-situ Measurement Setup and Measurement Conditions

5 to 100 mg of powdered catalyst was pressed into a disk (20 mm diameter), which was placed in the center of a variable temperature (-180 to 650 ˚C) IR cell. The cell is connected to a system that can be evacuated and introduced various gaseous molecules. Pretreatment was conducted by thermal evacuation to eliminate adsorbed water before measurements. NaCl or KBr windows are generally used for mid-IR spectroscopy, but polyethylene windows are used for far-IR spectroscopy. Polyethylene windows require a certain thickness to be resistant for evacuation at high temperatures, but thicker windows reduce the transmitted light intensity in a trade-off manner. So, 2.0 mm was selected as the optimal thickness. Temperature could be controlled from -100 to 400 ˚C. A 5 μm mylar beam splitter and PE-TGS detector were used to obtain averaged spectra of 256 integrations at 4 cm^{-1} resolution.

4. Far-IR Spectra of Alkali Ion Exchange Type FAU Zeolite (Y5.6)

When the proton is the cation (HY5.6 zeolite), a band attributed to acidic OH groups is observed in mid-IR at 3547 cm^{-1}, and no absorption appears in the far-IR region as shown in the bottom spectra of Fig. 4. (The band at 3640 cm^{-1} is due to OH-stretching vibration of silanol SiOH groups present on the external surface of the zeolite.) In cases where protons of HY5.6 zeolite were ion-exchanged with various alkali ions, absorption bands in the mid-IR region disappeared, but alternative absorption bands appeared in the far-IR region at different frequencies depending on the type of cation masses. Assuming a diatomic molecule with masses of m_1 and m_2, the IR absorption energy is estimated by using Hooke's law indicated below and shifted according to the effective mass μ, where $\tilde{\nu}$, π and k are the vibrational frequency, pi and the spring constant, respectively.

$$\tilde{V} = \frac{1}{2\pi}\sqrt{\frac{k}{\mu}}\ ,\quad \mu = \frac{m_1 m_2}{m_1 + m_2}$$

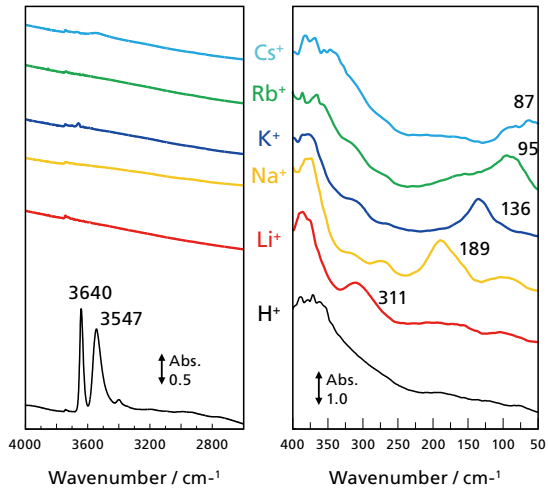

Fig. 4 Far-IR Spectra of Alkali Metal Ion-Exchange Y5.6 (FAU Type) Zeolite

Considering the hydroxyl groups on a solid surface, for example, when the OH groups are isotope-exchanged to OD groups, the vibrational isotope ratio becomes 1.41^{-1} ($1/\sqrt{2}$), assuming that lattice oxygens are fixed and that only H or D atoms are responsible for vibration. On the other hand, if OH and OD groups are regarded as diatomic molecules, then the isotope ratio is calculated to be 1.37^{-1}. For acidic OH groups on zeolites, experimentally measured vibration frequencies are 3547 cm^{-1} for OH groups, 2688 cm^{-1} for OD, indicating a 1.32^{-1} ratio between them, which is lower than the predicted values. In other words, the difference between calculated mass values is less than the calculated difference (contribution of H and D to the effective mass is low). Consequently, for solid surface species, not only the lattice oxygen and hydrogen atoms but presumably also the mass of zeolite skeletal structures is somewhat involved.

If the mass dependence of the simple cation vibration is applied to the frequencies observed in Fig. 4, the absorption would appear by the replacement of hydrogens to respective ions in the range from 1370 to 313 cm^{-1} ($Li \rightarrow Cs$), which differs significantly from experimental values. However, if Hooke's law is applied with Na^+ as a standard, results closely match experimental results [13] in cases where masses of individual cations alone are considered rather than the effective mass calculated from a lattice oxygen and alkali metal ion. Therefore, it is reasonable to attribute the observed absorption to the vibration of individual alkali metal ions located within the electrostatic field of the zeolite lattice, so-called cation vibration (Fig. 5).

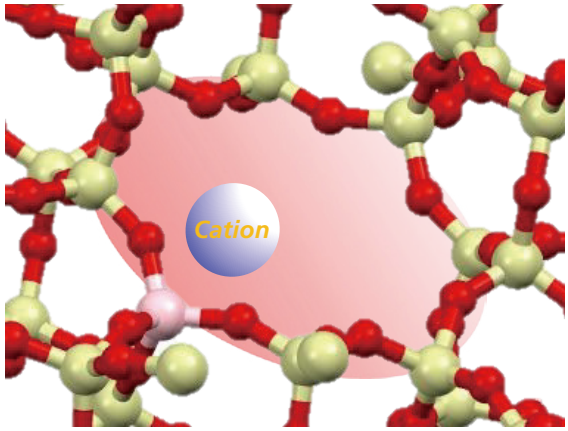

Fig. 5 Cation Vibration in the Electrostatic Field of a Zeolite Lattice

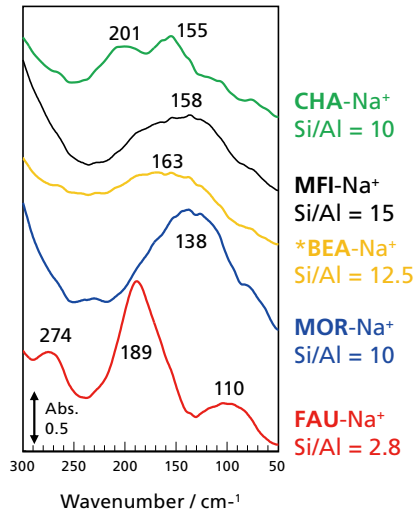

Fig. 6 Comparison of Na^+ Cation Vibration for Different Skeletal Structures

5. Far-Infrared Spectra of Cation Vibration in Different Zeolite Structures

Next, cation vibration of a fixed cation in zeolites with different topologies, or in other words different internal pore structures, was considered. Fig. 6 compares cation vibrations in 5 types of Na^+ ion-exchanged zeolites. CHA and FAU types have cage structures (caged spaces), whereas MFI, BEA*, and MOR types are composed of channel structures. Because the higher cation density facilitates the spectral observation, samples with high Al contents (low Si/Al ratio) were used. Though the samples differed not only in absorption frequency (energy) but also in the number of absorption peaks (to be more accurate, the absorption also differed in peak width, intensity, and other characteristics), sufficient experimental information was not provided for detailed discussions. Note that similar results as those shown in Fig. 4 were also obtained from CHA-type zeolites with various types of cations, indicating the same type of first-order dependence on $(1/\sqrt{m})$, where m is the cation mass, similarly to FAU type zeolites. Thus, cations inside zeolite pores, not limited to FAU type zeolites, are confirmed to vibrate as point charges within an electrostatic field formed by lattice oxygens. These results also indicate that the mass dependence of cations (the dependence of the vibration frequency on $1/\sqrt{m}$) differed for FAU and CHA-type zeolites. Therefore, the electrostatic fields generated by the pores consisting of lattice affect the interaction between the electrostatic field and cation, resulting in the difference in cation vibration energy (frequency).

6. Vibration Spectra of Molecular Cations

Though thermal evacuation was performed to eliminate adsorbed water from the ion-exchanged zeolite, such static measurements are far from so-called in-situ observation, which trace the behavior upon atmospheric changes. So, molecular cations were used to verify absorption peaks by dissociation/desorption of molecular cations by thermal evacuation and the successive adsorption of basic molecules. Fig. 7 shows spectral changes of NH^{4+} form FAU-type (Si/Al = 2.8) and CHA-type (Si/Al = 10) zeolites by treatments under various conditions. First, a, NH^{4+}–FAU zeolite absorption band due to ammonium cations was observed at 176 cm^{-1} after evacuation at 70 ˚C, but it disappeared at 250 ˚C under evacuation. Temperature-programmed desorption of ammonia and mid-IR spectroscopy confirmed the thermal desorption of ammonia from the NH^{4+} type zeolite, generating a proton form zeolite from the ammonium-type. Therefore, the absorption band, which disappeared at that temperature, is fairly attributed to ammonium cations. When a small amount of ammonia was then added at room temperature, the disappeared peak was again observed and the original state was eventually restored, which verified the attribution indicated above. Furthermore, when pyridine was added after the ammonia desorption, the absorption band appeared at a different frequency (137 cm^{-1}), which indicates that vibrational absorption is also observed for molecular cations in the same manner as that for alkali cations.

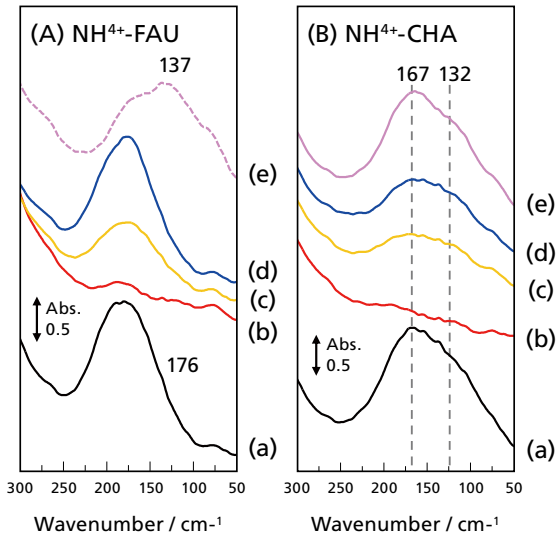

Fig. 7 Far-IR Spectra of NH^{4+} Zeolite after Thermal Evacuation, Re-adsorption of NH_3, and Adsorption of Pyridine

(A) (a) evacuation at 70 ˚C, (b) evacuation at 250 ˚C, (c) (b) after adsorption of NH_3 (135 Pa), (d) (b) after NH_3 (540 Pa) adsorption and (e) (b) after pyridine (500 Pa) adsorption

(B) (a) evacuation at 70 ˚C, (b) evacuation at 250 ˚C, (c) (b) after NH_3 (270 Pa) adsorption, (d) (b) after NH_3 (810 Pa) adsorption, and (e) (d) heated to 100 ˚C

Helium dilution gas (27 %) was used for NH_3 supply, and all spectra were measured at room temperature.

Next, a CHA-type zeolite with small-diameter (0.38 nm × 0.38 nm) cage-type pores (Fig. 7 (B)) was observed. The absorption bands observed after evacuation at 70 ˚C (at 167 cm^{-1} and 132 cm^{-1}) disappeared at 250 ˚C for the CHA-type zeolite, but the bands were not completely recovered by the ammonia supply at room temperature. However, the spectrum was restored by heating the sample to 100 ˚C in the presence of the added ammonia. It is due to the thermal excitation of lattice vibration (pore mouth breathing) at 100 ˚C, which effectively enlarges the pore opening size, that ammonia molecules, which could not adequately enter the pores at room temperature, were able to access the acidic sites (OH groups) inside pores to restore the original NH^{4+}–CHA zeolite form.

7. Specificity for Zeolite Solid Acid Catalysts (Fig. 8)

The observation of cation vibration within zeolite pores, as described in this article, verified the conventional wisdom that "zeolites form covalent bonds as acidic OH groups when cations are H^+, whereas alkali meta-exchanged zeolites are stabilized by the delocalized negative charge over the overall lattice." In combination with other zeolite properties observed previously, the above results were compared to the acid-base properties of other oxide catalysts. Using CO_2 as a probe to evaluate the basicity of the lattice oxygen in a protonic zeolite, it was found that the oxygen atoms bound to Al in the vicinity of acidic OH groups had basicity [12]. It is also reported that some catalytic reactions proceed at an acidic OH group and a basic lattice oxygen as a Brønsted acid-base pair [8, 9].

These results resemble the Lewis acid-base pair sites consisting of metal cations and lattice oxygens on metal oxide surfaces, which promote many catalytic reactions in concerted manners. In light of the mobility of the surface OH group, they are considered to migrate on the surface of oxides either as atomic hydrogen or as protons at high temperatures since the isolated OH groups on oxides are dehydrated when heated at 600 °C or above. In the case of zeolites, on the other hand, protons migrate at a low temperature above 100 ˚C [11], over the delocalized negative charge of lattice oxygens by formatting "proton and lattice" acid-base pairs. The observation of cation vibrations at room temperature further supports the facile delocalization of negative charges on zeolites. While active sites are separated on flat solid surfaces, where the delocalization of charges only occurs at a very high temperature range, active sites are concentrated in the three-dimensional space of porous structures like zeolites, which encourages the charge delocalization over a broad area. This is regarded as one of the key factors that enables zeolites to exhibit high catalytic activities (reactions progress at low temperatures).

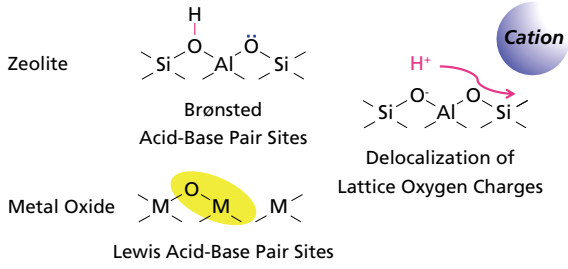

Fig. 8 Active Sites on Solid Catalyst Surface of Oxides

8. Conclusion

Some parallel research topics during the absence of any data from the present study, brought additional important information for a deeper understanding of zeolite chemistry: why zeolites, unlike other acid-base catalysts, are so special. Thus, such consideration is mentioned at the end of this article.

Research using far-IR spectroscopy has not produced sufficient results yet, which admittedly leaves a sense of something being left. Especially for molecular cations, the position of charges within the molecule needs to be considered in addition to their mass. Consequently, the discussion of results was not sufficient. The author hopes for a significant increase in research using far-IR spectroscopy in the future. For those interested in a more detailed data analysis of cation vibrations mentioned in this article, references are provided below.

References

[1] D. Hoge, M. Tüshaus, E. Schweizer, A. M. Bradshaw, The metal-carbon stretch in the vibrational spectrum of CO adsorbed on Pt (111), *Chem. Phys. Lett*., **1988**, 151, 230-235.

[2] I. J. Malik, M. Trenary, Infrared reflection-absorption study of the adsorbate-substrate stretch on Pt(111), *Surf. Sci*., **1989**, 214, L237-L245.

[3] C. Pazé, S. Bordiga, C. Lamberti, N. Salvalaggio, A. Zecchina, G. Bellussi, Acidic Properties of H-β Zeolite as probed by bases with proton affinity in the 118–204 kcal mol-1 range: A FTIR investigation, *J. Phys. Chem. B*, **1997**, 101, 4740-4751.

[4] J. N. Kondo, K. Domen and F. Wakabayashi, IR study of adsorption of olefins on deuterated ZSM-5, *J. Phys. Chem. B*, **1998**, 102, 2259-2262.

[5] R. Osuga, T. Yokoi, J. N. Kondo, IR observation of activated ether species on acidic OH groups on H-ZSM-5 zeolites, *Molecul. Catal*., **2019**, 477, article number 110535.

[6] J. N. Kondo, K. Domen and F. Wakabayashi, IR study of reaction of 2-butene adsorbed on deuterated ZSM-5 and mordenite, *Catal. Lett*., **1998**, 53, 215-220.

[7] H. Ishikawa, E. Yoda, J. N. Kondo, F. Wakabayashi and K. Domen, Stable dimerized alkoxy species of 2-methylpropene on mordenite zeolite studied by FT-IR", *J. Phys. Chem. B*, **1999**, 103, 5681-5686.

[8] H. Yamazaki, H. Shima, H. Imai, T. Yokoi, T. Tatsumi, J. N. Kondo, Evidence for "carbene-like" intermediate during the reaction of methoxy species with light alkenes on H-ZSM-5", *Angew. Chem. Int. Ed*., **2011**, 50, 1853-1856.

[9] J. N. Kondo, H. Yamazaki, R. Osuga, T. Yokoi, T. Tatsumi, Mechanism of decomposition of surface ethoxy species to ethene and acidic OH groups on H-ZSM-5, *J. Phys. Chem. Lett*., **2015**, 6, 2243-2246.

[10] J. N. Kondo, H. Yamazaki, T. Yokoi, T. Tatsumi, Mechanisms of reactions of methoxy species with benzene and cyclohexane over H-ZSM-5 zeolites, *Catal. Sci. Technol*., **2015**, 5, 3598-3602.

[11] R. Osuga, T. Yokoi, K. Doitomi, H. Hirao, J. N. Kondo, IR investigation of dynamic behavior of Brønsted acid sites on zeolites at high temperatures, *J. Phys. Chem. C*, **2017**, 121, 25411-25420.

[12] R. Osuga, T. Yokoi, J. N. Kondo, Probing the basicity of lattice oxygen on H-form zeolites using CO_2, *J. Catal*., **2019**, 371, 291-297.

[13] R. Osuga, T. Yokoi, J. N. Kondo, In-situ far-IR study of vibrations between zeolite frameworks and metallic or molecular cations, *Micropor. Mesopor. Mater*., **2020**, 305, 110345.

[14] Y. Ikemoto, M. Ishikawa, S. Nakashima, H. Okumura, Y. Haruyama, S. Matsui, T. Moriwaki, T. Kinoshita, Development of scattering near-field optical microspectroscopy apparatus using an infrared synchrotron radiation source, *Opt. Commun*., **2012**, 285, 2212-2217.

[15] F. M. Hoffmann, Infrared reflection-absorption spectroscopy of adsorbed molecules, *Surf. Sci. Rep*., **1983**, 3, 107-192.

[16] Y. J. Chabal, Surface infrared spectroscopy, *Surf. Sci. Rep*., **1988**, 8, 211-357.

[17] H. Esemann, H. Förster, E. Geidel, K. Krause, Exploring cation siting in zeolite ZSM-5 by infrared spectroscopy, EXAFS and computer simulations, *Micropor. Mater*., **1996**, 6, 321-329.

[18] Y. Ikemoto, T. Moriwaki, T. Nakano, Y. Nozue, Far infrared microscopy of zeolite MOR single crystal, *Infrared Phys. Technol*. **2006**, 49, 78-81.

[19] H. Esemann, H. Förster, Joint X-ray absorption and far infrared spectroscopic studies on zeolite surfaces – exchange and siting of copper ions and their redox behavior during NO decomposition in zeolite ZSM-5, *J. Mol. Struct*., **1999**, 482-483, 7-11.

Infrared Microscope Detectors

Spectroscopy Business Unit, Analytical & Measuring Instruments Division
Shinya Wakuda

1. Introduction

In terms of Shimadzu infrared microscopes, the AIRsight infrared/Raman microscope was released in November 2022 and the AIMsight infrared microscope was released in February 2023, as the successor to the AIM-9000 model (Fig. 1). Both microscopes use a Type II Super Lattice Infrared Detector (T2SL) that detects infrared quanta as the standard detector for infrared measurements. T2SL detectors are able to detect infrared light variations with high sensitivity, which is necessary for measuring micro areas, by cooling the detector element with liquid nitrogen. Though such detectors may be necessary for measuring micro areas with high sensitivity, there has been increasing resistance to using liquid nitrogen, due to the risk of oxygen deficiency caused by evaporated liquid nitrogen in closed rooms or serious low-temperature burns or frostbite from liquid nitrogen contacting the skin. Therefore, optional thermoelectrically cooled mercury cadmium telluride (TEC MCT) detectors, which do not require liquid nitrogen and are also capable of measuring 25 µm-square micro areas, have been offered since January 2025. This article describes the characteristics of both types of detectors. A DLATGS detector is also available for room temperature measurements up to 400 cm^{-1}.

2. T2SL Detectors

T2SL detectors are quantum detectors for measuring infrared light. They consist of over 2,000 alternating layers of indium arsenide (InAs) and gallium antimonide (GaSb) films a few nanometers thick configured into a so-called super lattice structure. Due to the unique structure of T2SL detectors, they have a broader band up to the 14.5 µm (690 cm^{-1}) cut-off wavelength and achieve sensitivity that is helpful for measurements within micro areas. In addition, because T2SL detectors do not contain any mercury or cadmium, which are restricted by the European Union (EU) Restriction of Hazardous Substances in Electrical and Electronic Equipment (RoHS), the expectation is that they will replace mercury cadmium telluride (MCT) detectors, which are commonly used in infrared microscopes, because MCT detectors contain hazardous substances.

Fig. 1 AIRsight (Left) Infrared/Raman and AIMsight (Right) Infrared Microscopes
(Both Configured with IRXross FTIR Spectrophotometers)

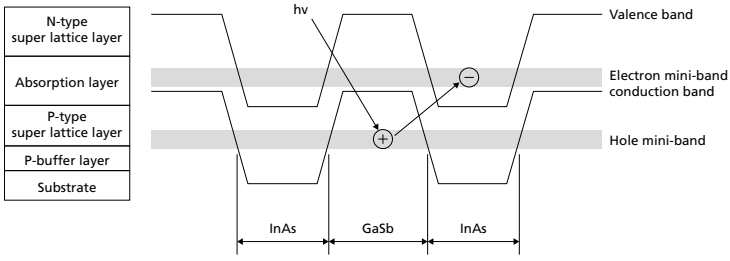

Fig. 2 Cross-Section Diagram of Super Lattice Structure and Energy Levels

Table 1 Measurement Conditions

Detector: Instrument	T2SL: IRXross, AIMsight MCT: IRTracer-100, AIM-9000
Measurement Mode	Transmission
Aperture	50×50 μm
Resolution	8 cm^{-1}
Number of Scan	45 times
Apodization Function	SqrTriangle
Detector	T2SL, MCT

Fig. 2 illustrates the cross-section of a super lattice structure and corresponding energy levels.

In T2SL detectors, the stack of alternating InAs and GaSb thin films results in forming energy bands (electron and hole mini-bands) that are not present in bulk crystals. By controlling the corresponding energy level, the detector can achieve a narrower band gap. For example, even if using the same InAsSb compound for the semiconductor photodetector, changing the ratio of In, As, and Sb elements will change the band gap, which can result in changing the cut-off wavelength. However, though the cut-off wavelength can be broadened by narrowing the band gap, doing so will also increase noise-causing dark current levels due to higher thermal excitation. Consequently, for InAsSb detectors, the cut-off wavelength can only be broadened up to 12 μm (833 cm^{-1}), which is inadequate for use in infrared microscopes. In contrast, with T2SL detectors, even if the band gap is narrow, the band structure formed by the electron and hole mini-bands, as shown in Fig. 2, allows the hole and electron recombination rate to be controlled to inhibit dark currents that can increase noise-causing thermal excitation. That means the T2SL detector cut-off wavelength can be increased to 14.5 μm and the detector can achieve the high signal-to-noise (S/N) ratio necessary for infrared microscopes (equivalent to the S/N ratio of MCT detectors).

T2SL detectors also provide linearity that is superior to MCT detectors. Photoconductive MCT detectors detect variations in electrical conductivity based on variations in the carrier (electrons/holes). That makes the detectors easily affected by recombination or movement of the carrier and makes them prone to losing linearity. In contrast, photovoltaic T2SL detectors directly detect variations in current generated by the carrier and, with a super lattice structure that can be used to control carrier recombination, they can maintain high linearity.

As a specific example, two different types of detectors (T2SL and MCT) were used to measure transmittance through a stack of 1 to 7 layers of 6 μm thick PET (polyethylene terephthalate) film. The measurement conditions are indicated in Table 1.

Infrared spectra obtained with an IRXross/AIMsight (T2SL detector) system are shown in Fig. 3, whereas infrared spectra obtained with an IRTracer-100/AIM-9000 (MCT detector) are shown in Fig. 4.

The extremely strong absorption from C-O stretching vibration (1,240 cm^{-1}) in aromatic esters indicates that peak tops from the MCT detector became saturated from near where Abs exceeds 1.5. When a large amount of light enters an MCT detector, the output becomes saturated, so that absorbance is no longer proportional to concentration. In contrast, for the T2SL detector, absorbance increases up to nearly Abs = 2.5, which means it can detect peaks more accurately.

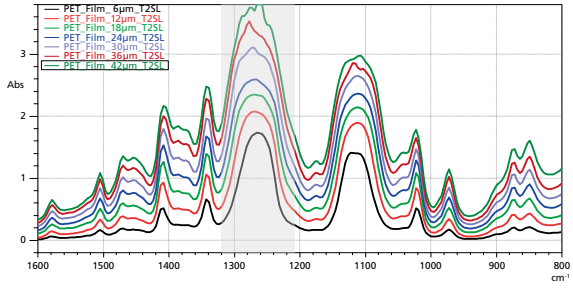

Fig. 3 Measurements Using IRXross/AIMsight (T2SL Detector) System
Infrared Spectra of 6 μm Thick PET Film (Transmittance Measured through Stack of 1 to 7 Layers)

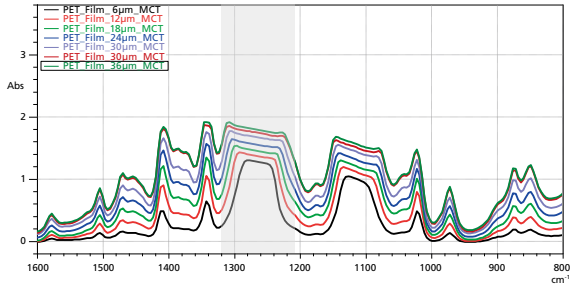

Fig. 4 Measurements Using IRTracer-100/AIM-9000 (MCT Detector) System
Infrared Spectra of 6 μm Thick PET Film (Transmittance Measured through Stack of 1 to 7 Layers)

Noting the slightly weaker peaks (1,340 cm^{-1}) characteristic of crystalline PET, the linearity with respect to the number (thickness) of stacked layers was checked. Calibration curves were calculated from the height of corresponding peaks using the linear multi-point calibration curve method (without baseline correction or using the origin point). Calibration curves obtained with the T2SL and MCT detectors are shown in Fig. 5. Using the T2SL detector resulted in a high coefficient of correlation of r2 = 0.994 for transmittance measurements through a stack of film 42 µm thick (7 layers). In contrast, with the MCT detector, linearity dropped significantly beyond a thickness of 24 µ m (4 layers).

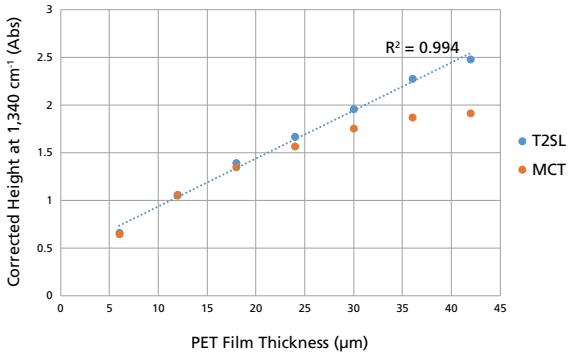

Fig. 5 Corrected Height of Peaks at 1,340 cm^{-1} for Various PET Film Thicknesses

Though peak intensity for transmission and reflection methods is generally proportional to the sample thickness, high light input levels result in lower linearity from the MCT detector than with T2SL detector, with peak saturation presumably occurring from about Abs = 1.5 absorbance levels.

Thus, T2SL detectors offer the advantage of being able to acquire better data than MCT detectors due to their lack of saturation over a broader range of concentrations (or thicknesses).

3. TEC MCT Detectors

Typically, infrared microscope models with a liquid nitrogen-cooled high-sensitivity infrared detector are used to measure micro areas. However, in an increasing number of cases in recent years, liquid nitrogen cannot be used at the intended facility or users are reluctant to use liquid nitrogen for safety reasons. Shimadzu offers an optional DLATGS detector for infrared microscopes that does not use any liquid nitrogen, but the smallest area size it can detect is about 100 µm square and it does not provide sufficient sensitivity for users who want to measure smaller micro areas without using liquid nitrogen. Therefore, a new optional TEC MCT quantum detector has been added to the product line.

TEC MCT detectors include an internal multistage Peltier element installed inside a CAN package type detector element that is controlled to a constant temperature by Shimadzu-designed temperature-control circuitry. An inert gas with low thermal conductivity is also sealed inside the detector element to prevent measurement errors, such as those caused by condensation. The TEC MCT detector features a photoconductor for detecting variations in the carriers (electrons/holes) mentioned above as variations in resistance. In order to detect the resistance variations, a bias current is applied and the corresponding voltage is detected, but applying the bias current when the MCT detector is not adequately cooled could damage the MCT detector. Therefore, Shimadzu systems are designed to continuously monitor the temperature to only apply a bias current when the temperature is appropriate and stabilized. In normal laboratory environments, the temperature stabilizes within a minute after switching the infrared microscope power supply ON.

Another feature of TEC MCT detectors is that the lens is molded into the detector surface, which increases the apparent area of the detector and allows the actual detector area to be designed smaller. A detector with an apparent area of 1 square millimeter is used, but the actual detector area is about 1/11th of the apparent area. In general, the specific detection capacity is defined by the D* value, as indicated by the following formula and described in FTIR TALK LETTER Vol. 13 "Using Infrared Detectors—MCT Detector—." The higher the D* value, the better the sensitivity, but as indicated in the formula, the D* value is inversely proportional to the detector area, so it is advantageous to have a smaller detector surface.

$$D^* = \frac{(S_V/N_V) \times (\Delta f)^{1/2}}{P \times A^{1/2}}$$

SV: Signal output (volts) [V]
P: Incident energy [W/Hz1/2]
A: Area of detector element light-receiving surface [cm^2]
NV: Noise output (voltage) [V]
Δf: Noise bandwidth [Hz]

The measurable sample sizes, S/N ratio, and measurable wavenumber range of each infrared microscope series detector used to measure transmittance are indicated in Table 2.

Table 2 Respective Detectors for Infrared Microscope Series

Instrument	Detector		Liquid Nitrogen	Object Sizes Measurable for Transmittance Measurements	S/N	Measurable Wavenumber Range
AIMsight AIRsight	Standard	T2SL	Required	Up to 10 µm	30,000:1	5,000 to 700 cm^{-1}
	Optional	TEC MCT	Not required	Up to 25 µm	2,000:1	
		DLATGS		Up to 100 µm	100:1	4,600 to 400 cm^{-1}

The following describes a specific example of measuring the same sample using the three detectors above. The sample is a polypropylene-based plastic used for automotive bumpers that contains magnesium silicate (TALC). The infrared spectra in Fig. 6 were obtained by placing the sample on a diamond cell, rolling it, and then measuring transmittance according to the measurement conditions in Table 3.

Table 3 Measurement Conditions

Instrument	IRTracer-100, AIMsight
Measurement Mode	Transmission
Aperture	25×25 µm
Resolution	8 cm^{-1}
Number of Scan	20 times (T2SL) 500 times (TEC MCT and DLATGS)
Apodization Function	Happ-Genzel
Detector	T2SL, TEC MCT, DLATGS

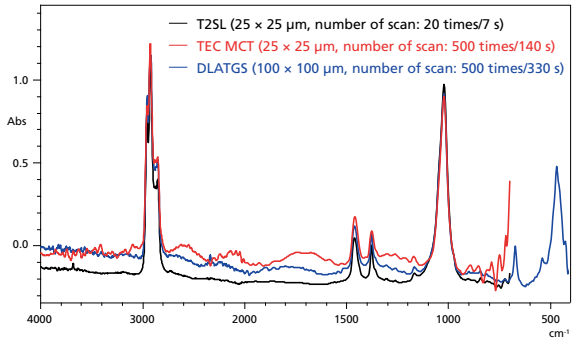

Fig. 6 Infrared Spectra of Polypropylene-based (containing TALC) Resin for Automotive Bumpers Using the Three Different Detectors

A comparison of the data from the T2SL and TEC MCT detectors shows that low-noise data can be acquired more quickly using the T2SL detector. However, it also shows that the TEC MCT detector provides more than adequate data for qualitative analysis of 25 × 25 µm micro areas.
A comparison of the data from the TEC MCT and DLATGS detectors shows that measurement times differ even for the same number of scans. That is because the DLATGS detector itself has frequency characteristics that require setting a slower scan speed than for quantum type T2SL and TEC MCT detectors. In addition, though they cannot measure smaller micro areas than T2SL and TEC MCT detectors, DLATGS detectors enable measurements up to the 400 cm^{-1} wavenumber range, which makes the qualitative analysis of certain inorganic compounds possible.
Therefore, the detector should be selected based on the purpose of analysis.

4. Conclusion

This article described new infrared detectors for Shimadzu infrared microscopes, including the liquid nitrogen-cooled T2SL detector and the thermoelectrically cooled MCT detector that does not use any liquid nitrogen. Hopefully, the article will be helpful for selecting a detector for infrared microscope measurements. Please consider using a Shimadzu AIMsight infrared microscope system or AIRsight infrared/Raman microscope system equipped with these detectors.

References

[1] Ko Kawane, Karen Maruyama, "Sensitivity Evaluation and Example Analysis of Microscopic Targets with Thermoelectrically Cooled MCT Detector," Shimadzu Application News 01-00826-EN (First Edition: January 2025)

Notes on Infrared Spectral Analysis —Carbonyls (Part 1)—

Solutions COE, Analytical & Measuring Instruments Division
Yoshiyuki Tange

1. Introduction

The previous issue of FTIR TALK LETTER (Vol. 43) included an article that presented notes on the infrared spectral analysis of aliphatic unsaturated hydrocarbons (olefins) and aromatics. As an application, it also described how to check for differences between cis and trans isomers of butadiene rubber based on their infrared spectra. This article discusses C=O stretching vibration in carbonyl groups (Part 1). C=O stretching vibration is known to be prone to peak shifting due to the effects from adjacent functional groups and other factors. Various examples are described below regarding the relationship between molecular structures around carbonyl groups and the peak positions of C=O stretching vibration.

2. Infrared Absorption of C=O Stretching Vibration

The presence or absence of carbonyl groups can be easily determined from looking at the infrared spectra acquired. That is due to the large infrared absorption by C=O stretching vibration and because almost no other infrared absorption by functional groups occurs within that same wavenumber range. Infrared spectra for several molecules that include carbonyl groups are shown in Fig. 1.

(1) Ketone
: 1,725 to 1,705 cm^{-1}
Acetone

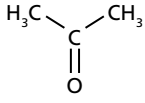

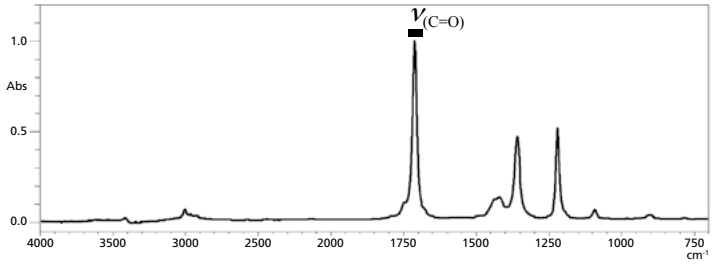

(2) Aldehyde
: 1,740 to 1,720 cm^{-1}
Acetaldehyde

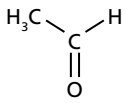

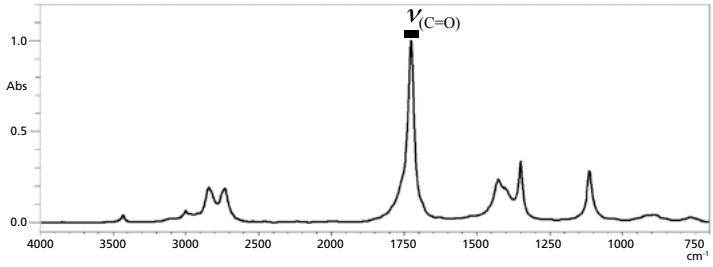

(3) Linear ester
: 1,750 to 1,735 cm^{-1}
Methyl Acetate

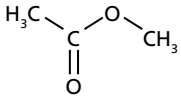

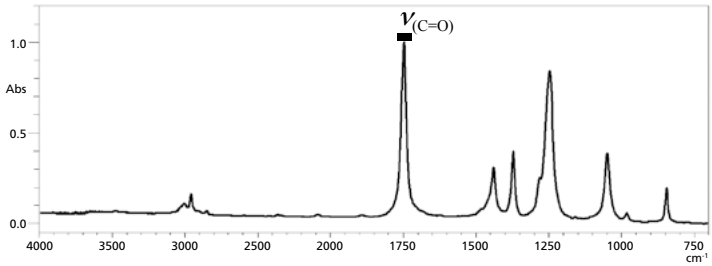

(4) Lactone (cyclic ester)
: 1,795 to 1,760 cm^{-1}
γ-Nonalactone

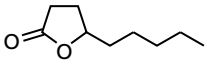

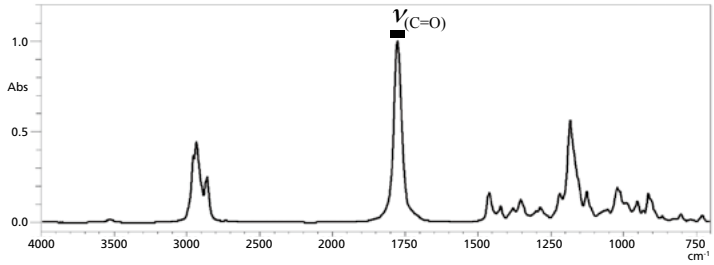

(5) Conjugate
: 1,700 to 1,670 cm^{-1}
Acetophenone

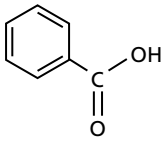

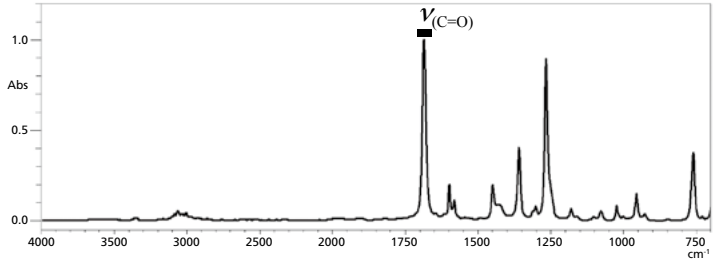

(6) Carboxylic acid
: 1,720 to 1,680 cm^{-1}
Heptanoic acid

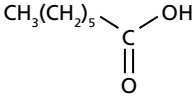

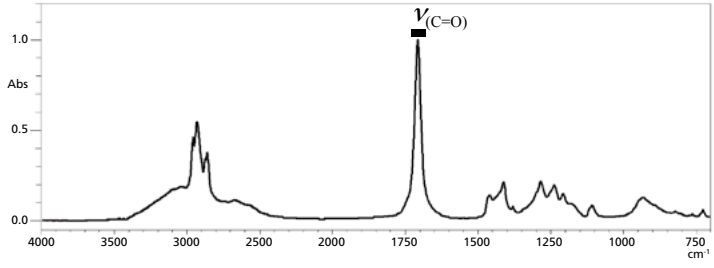

(7) Carboxylate salt
:1,650 to 1,540 cm^{-1}
1,450 to 1,360 cm^{-1}
Sodium Stearate

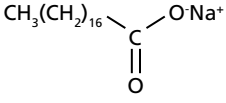

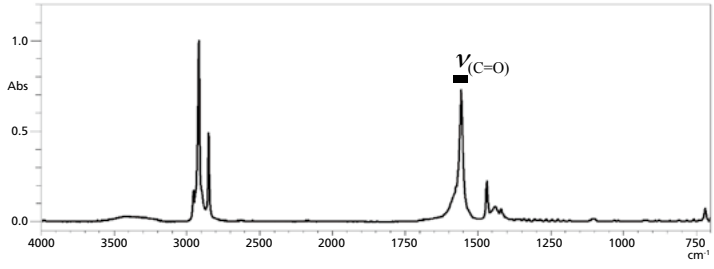

(8) Amide
: 1,695 to 1,630 cm^{-1}
Polyamides

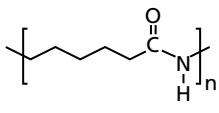

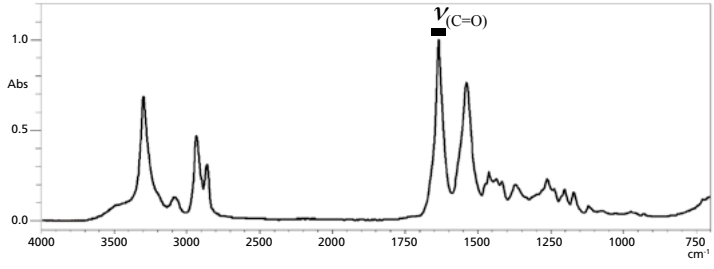

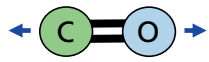

Stretching Vibration (ν)

Fig. 1 Infrared Spectra of Compounds with a Carbonyl Group [1]

3. Peak Positions of C=O Stretching Vibration Due to Adjacent Structures

The peak positions of carbonyl groups shift due to the effects from functional groups in adjacent positions. The following describes examples of shifting due to the masses and bond angles of adjacent functional groups, inductive effects, and resonance effects.

- **Mass Effects:**

(1) Ketone vs (2) Aldehyde

Peak position shifts due to masses are often explained by a comparison of hydrogen and deuterium atoms, where it is known that the heavier the mass, the farther the peak position shifts toward the low-wavenumber end. That phenomenon can also affect positions adjacent to carbonyl groups. As a specific example, the infrared spectra for acetone, which is a type of ketone, and acetaldehyde were compared (Fig. 2). Fig. 2 shows that the peak positions from C=O stretching vibration of acetone appear farther toward the low-wavenumber end than acetaldehyde, but the difference between those peak positions depends on whether the functional group adjacent to the carbonyl group is hydrogen (-H) with a mass of 1 or a methyl group (-CH_3) with a mass of 15 [1].

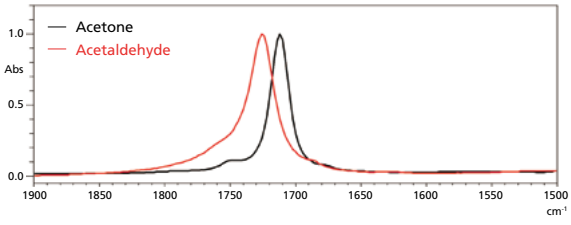

Fig. 2 Peaks from C=O Stretching Vibration of Acetone and Acetaldehyde

- **Bond Angle Effects:**

(3) Linear Ester vs (4) Lactone (Cyclic Ester)

In cyclic ketones, if the number of carbons forming cyclic rings decreases, then C=O stretching vibration is known to shift toward the high-wavenumber end. That is caused by distortion that occurs in the sp2 hybrid orbital of carbons in the carbonyl group [2]. More specifically, the normal 120-degree bond angle of the sp2 hybrid orbital increases due to the decrease in the number of cyclo-ring carbons. That results in distortion of the hybrid orbital [3] that shifts the peak position toward the high-wavenumber end. However, even if distortion occurs in the hybrid orbital, the coupling constant of double bonds in the carbonyl group are considered to remain unchanged [4].

Fig. 3 shows a summary of the peak positions for cyclic ketones with a different number of carbons in the cyclo-ring and for C=O stretching vibration. It shows how as the C-C=O bond angle increases, the peak position for C=O stretching vibration shifts toward the high-wavenumber end.

Fig. 4 shows a comparison of C=O stretching vibration peak positions for linear ester and lactone (cyclic ester). Just like for cyclic ketone, it shows the peak for the lactone with a larger bond angle shifted toward the high-wavenumber end.

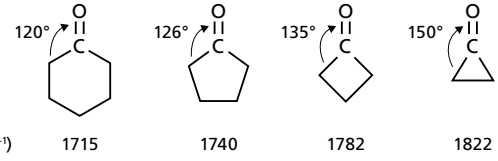

Fig. 3 Relationship between Bond Angle and C=O Stretching Vibration Peak Position[1]

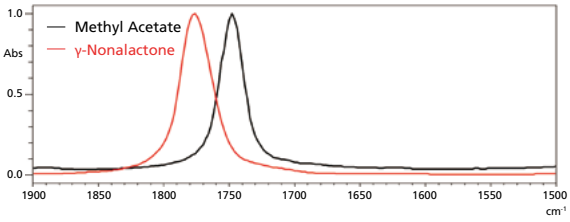

Fig. 4 Peaks for C=O Stretching Vibration of Methyl Acetate and γ-Nonalactone

- **Inductive Effects (I Effects):**

(1) Ketone vs (3) Cyclic Ester

The carbon and oxygen atoms in carbonyl groups are bound by strong σ bonds and weak π bonds. Normally, the π electrons in π bonds are attracted by oxygen atoms that have a large electronegativity, resulting in a weaker bond state than the original double-bond (Fig. 5).

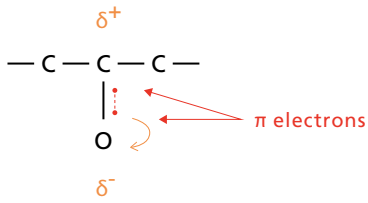

Fig. 5 Status of π Electrons in Carbonyl Groups

However, if an atom with high electronegativity, such as a halogen or oxygen atom, binds to the carbon atom bound to an oxygen atom, then the atom with high electronegativity will reduce the shift in the π electron position and increase the coupling constant of C=O stretching vibration (Fig. 6). That phenomenon is referred to as the inductive effect (I effect).

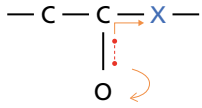

Fig. 6 π Electron Status in Carbonyl Groups if an Atom with High Electronegativity Binds to an Adjacent Position (X)

When the coupling constant in a carbonyl group increases due to the inductive effect, the peak position for C=O stretching vibration shifts toward the high-wavenumber end. Fig. 7 shows a comparison of C=O stretching vibration peak positions for ketone and ester. It shows how the I effect shifts the ester with an oxygen atom in an adjacent position farther toward the high-wavenumber end.

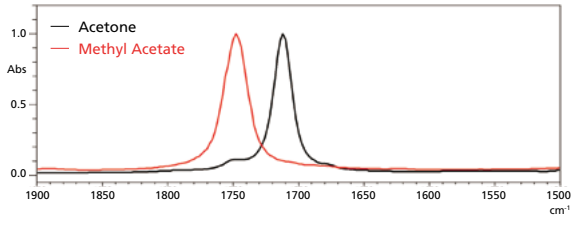

Fig. 7 Peaks from C=O Stretching Vibration of Acetone and Methyl Acetate

- **Mesomeric Effects (M Effects):**

(1) Ketone vs (5) Conjugate, (7) Carboxylate Salt, and (8) Amide

If there is a conjugate or an electron-releasing atom with an unshared electron pair in a position adjacent to a carbonyl group, then the C=O stretching vibration peak position will shift toward the low-wavenumber end.

Phenyl groups and vinyl groups are examples of adjacent structures with a conjugate. An example of acetophenone is shown in Fig. 8. The C=O coupling constant will decrease due to resonance with the structure that has reconnected π bonds.

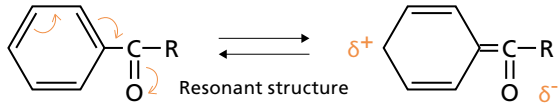

Fig. 8 Resonance in Acetophenone

If an atom with an unshared electron pair is present in an adjacent position, the unshared electron pair is transferred to an oxygen that forms the carbonyl group in order to decrease the C=O coupling constant and shift the C=O stretching vibration peak position toward the low-wavenumber end. For amide bonds, adjacent nitrogen atoms will have an I effect that shifts the C=O stretching vibration peak position toward the low-wavenumber end (Fig. 9).

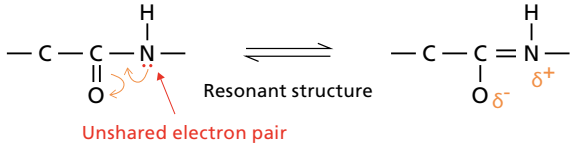

Fig. 9 Resonance in Amides

Halogen atoms and oxygen atoms can also have unshared electron pairs, but both have high electronegativity that tends to prevent them from achieving a positive static charge, which means the I effect is more dominant than the M effect. However, in the case of carboxylate salts, the oxygen atom present in a position equivalent to a carbonyl group causes a mesomeric effect that shifts the C=O stretching vibration peak toward the low-wavenumber end (Fig. 10).

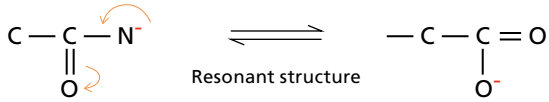

Fig. 10 Resonance in Carboxylate Salts

Fig. 11 shows a comparison of C=O stretching vibration peak positions for a ketone, conjugate system, amide, and carboxylate salt. It shows that for all the structures, the mesomeric effect results in the C=O stretching vibration peaks appearing farther toward the low-wavenumber end than the ketone.

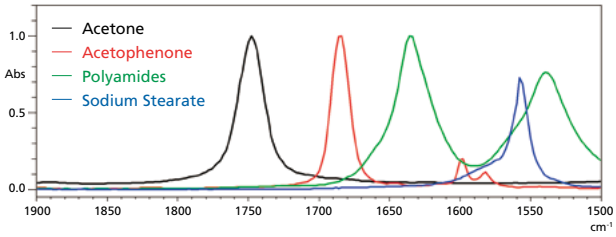

Fig. 11 Peaks from C=O Stretching Vibration of Acetone, Acetophenone, Polyamide, and Sodium Stearate

4. Conclusion

This article discussed the peak positions of C=O stretching vibration in several molecules that include carbonyl groups.

- C=O stretching vibration can often be clearly identified without overlapping other functional group peaks.
- The position of peaks from C=O stretching vibration can shift due to structures or atoms adjacent to the carbonyl group.
- Causes of peak shifting include the mass of adjacent structures, bond angle, inductive effects, and mesomeric effects.

The content of this article was limited to peak positions corresponding to C=O stretching vibration, but a future article will consider several molecules that contain carbonyl groups, how to discriminate the C=O stretching vibration peaks from peaks for other functional groups, and practical infrared spectral data analysis methods.

References

[1] Larkin P.J. Infrared and Raman Spectroscopy: Principles and Spectral Interpretation, Elsevier (2011)
[2] Shigeyuki Tanaka, Takuma Oba, Shozo Toda, "Actual Examples of Infrared Absorption Spectroscopy"-Fundamentals and Applications-," Hirokawa Publishing Co. (1964)
[3] Bellamy, Infrared Spectra of Complex Molecules, Methuen, (1958)
[4] N. B. Colthup and M. K. Orloff, Chem. Phys. Lett. 19, 298 (1973)

Shimadzu Corporation
www.shimadzu.com/an/